Observation of nonstandard Fickian diffusion at the interface of isotopically pure amorphous ^{11}B on ^{10}B by neutron reflectometry

S. M. Baker,* G. S. Smith, N. J. S. Brown,* M. Nastasi, and K. Hubbard
Los Alamos Neutron Scattering Center H-805, Los Alamos National Laboratory, Los Alamos, New Mexico 87545
(Received 9 September 1996)

As part of a larger study to investigate atomic-diffusion behavior in both elemental boron and refractory transition-metal borides, neutron reflectometry was used to examine the temperature-induced self-diffusion of isotopically enriched thin films of amorphous ^{11}B on ^{10}B deposited by electron-beam evaporation. The reflectometry studies were performed and model boron density profiles for samples annealed at various times and temperatures of 360 and 400 °C were fit to the reflectivity data. Although the $^{10}B/^{11}B$ interface did not move relative to the air/boron interface upon annealing, the expected standard Fickian diffusion for the annealed samples was not observed. A pinned Fickian diffusion model, which imposes the boundary conditions of a fixed composition of ^{10}B to ^{11}B at the interface, fit the reflectivity data accurately and consistently. A typical equilibrium diffusion constant was determined to be $\sim 10^{-17}$ cm^2 s^{-1}, measured at an annealing temperature of 360 °C. The measured diffusion constants are inconsistent with the high melting temperature of elemental boron, but are consistent with measured boron diffusion constants in other amorphous thin films. The presence of clusters in the boron film is proposed to explain the observed results. [S0163-1829(97)04611-0]

I. INTRODUCTION

Passivation of the surface of semiconductor devices has been achieved by coating them with thin films of insulating diborides.[1–3] While these films are chemically and mechanically stable at ambient temperatures, boron diffusion into the device at elevated temperatures is a possible side effect of such passivation. We became involved in a larger study of diboride diffusion into semiconductors by first examining the diffusion properties of elemental boron.

We began the study previously with the self-diffusion of amorphous, isotopically enriched ^{10}B on ^{11}B on silicon substrates.[4] The two boron isotopes have nearly identical chemical properties but significantly different neutron-scattering lengths, which gives the atoms ideal contrast for neutron-scattering techniques. These thin films ($\sim$700 Å of ^{11}B on 1400 Å of ^{10}B on silicon) were annealed for various times at 360 °C, and examined by neutron reflectometry (NR). We observed[4] that the reflectivity data obtained could not be modeled by the predicted standard Fickian model for diffusion at the interface. Interestingly, using a nonstandard pinned Fickian model for diffusion that assumes a fixed composition at the interface, we could obtain excellent fits to our reflectometry data. The fits converged onto a fixed isotope composition (ratio of ^{10}B to ^{11}B) at the interface independent of annealing time. The film thicknesses decreased by less than 6% upon initial annealing, and remained at a constant thickness upon any subsequent annealing. Furthermore, the diffusion constants obtained from the fits were nearly equal for each of the various annealing times, and on the order of 10^{-1} Å^2 s^{-1} (10^{-17} cm^2 s^{-1}) at 360 °C, consistent with boron diffusion in other amorphous materials.[5]

However, we were somewhat concerned that these results were an artifact of the deposition procedure. For the deposition of this first sample set (set A) discussed above, the shutters on the evaporation system were not fully operational, and thus the time between the application of the ^{11}B film on the ^{10}B film was 2–3 min. At 10^{-8} Torr, sufficient partial pressures of reactant gases such as oxygen may have been present in our chamber to form a monolayer or greater of contaminant at the interface. In order to test this possibility, the experiment was repeated on samples whose exposure to background contaminants was minimized (set B).

In this paper, we present the results of NR measurements on both sets of samples, and a comparison of these results. We discuss the implications of the pinned Fickian model on the measured diffusion constant, and propose the existence of nanocrystals or clusters to account for these observations. Finally, we discuss in detail the parameters that affect the magnitude of the difference between the diffusion constants obtained from the different models.

II. EXPERIMENTAL PROCEDURES

A. Sample preparation

All samples were prepared as described in Ref. 4 except for the differences noted below. The samples consisted of an amorphous bilayer of ^{11}B on ^{10}B on silicon. These substrates were 2.5×2.5-cm^2 squares cut from 6.4-mm-thick polished silicon discs. After thoroughly degreasing the substrates, the bilayers were prepared by electron-beam evaporation at 5×10^{-8} Torr of $\sim$1350 Å of ^{10}B onto the silicon substrates followed by deposition of $\sim$700 Å of ^{11}B. The samples were deposited four at a time, and rotated during the deposition in order to ensure uniformity. The boron deposition rate was $\sim$3 Å/s. For a contaminant at the stated pressure, the time required for ideal monolayer formation was $\sim$44 s. All depositions were made with the substrates at ambient temperature. The enrichment of the boron isotopes was given by the supplier (Eagle-Picher Industries, Quapaw, OK) as 93.64% for ^{10}B and 97.48% for ^{11}B. These values were consistent with secondary-ion-mass-spectroscopy (SIMS) measure-

ments. After the depositions, the samples were moved to a vacuum oven and annealed at a pressure of 1.5×10^{-8} Torr. All of the samples which were prepared during one evaporation were annealed at the same temperature; therefore, there were generally four samples per annealing temperature. A number of samples from different depositions were prepared and not annealed.

For set A, the elapsed time between the ^{10}B and ^{11}B depositions was 2–3 min. The annealing times and temperatures analyzed were 0.0, 2.4, 5.4, 9.7, 22.3, and 35.4 h, and 0.0, 0.5, 1.0, and 2.0 h for the 360 and 400 °C anneals, respectively. In the case of the 360 °C annealed samples, the reflectivity curves were measured on the first four specimens, and then the 0.0- and 2.4-h annealed samples were further annealed to produce the 22.4- and 35.4-h annealed samples. For set B, the ^{11}B deposition followed the ^{10}B deposition within a matter of 3–5 s as opposed to 2–3 min. Individual set B samples were annealed in a vacuum oven at 360 °C for 0.0, 5.0, 10.4, and 23.4 h. Note that one sample of this set was left annealed.

B. Neutron reflectivity measurements

Like the reflection of light from interfaces with different indices of refraction, neutrons reflect and refract at interfaces with different neutron-scattering length densities. Because the interaction is a short-range nuclear interaction ($\sim10^{-15}$ m) that does not depend on the electron density, neutrons can have significant scattering from both light and heavy nuclei. Furthermore, differences in neutron-scattering length between isotopes can be substantial, leading to the unusual ability to differentiate between electronically similar species such as deuterium and hydrogen, and in this case, between ^{10}B and ^{11}B. By defining the neutron energy and the angle incident to the surface, a momentum transfer perpendicular to the surface can be determined for the interaction of a neutron and a particular interface. Using the same mathematics used in the reflection of light, interpretation of interference patterns for specular neutron reflectivity can be determined. For example, for a single thin film, the peak heights on a plot of reflectivity (R is the number of reflected neutrons divided by the number of incident neutrons) vs momentum transfer are related to the magnitude of the scattering length difference between thin film and surface, and the peak separation is related to the thickness of the thin film.

For more complicated interfaces, such as the diffusion of a particular type of atom or molecule, obtaining a density profile of the substance in question perpendicular to the surface is the goal. Since each element in the density profile contributes to the overall scattered intensity at a given wavelength, an inverse problem results. The common solution to this problem is to develop a theoretical model of the profile, and to do a nonlinear least-squares fit of the resultant calculated reflectivity curve with the experimental data. The result is that, as in any inverse problem, the fit is very sensitive to abrupt changes in slope or dramatic differences of density at an interface, in addition to smaller changes seen as an atom diffuses. Analysis of diffusion is straightforward, as long as the diffusing material and substrates have significantly different neutron-scattering length densities. An excellent review of the technique of neutron reflectivity, a number analytical approaches, and experimental examples can be found in Ref. 6.

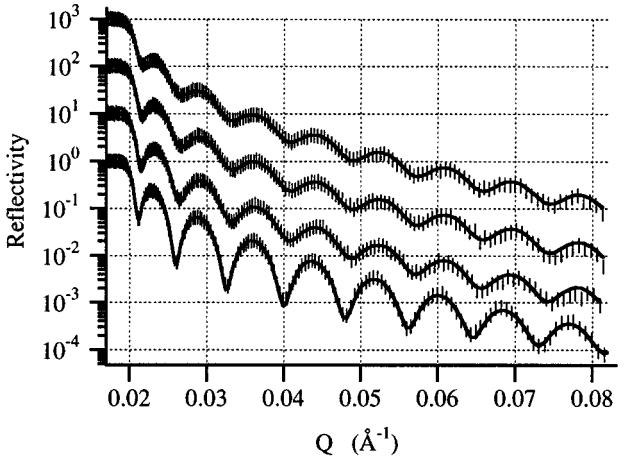

FIG. 1. Neutron reflectivity plotted vs the perpendicular momentum transfer Q_z, as explained in the text. Experimental data are represented by vertical lines (error bars too small to be seen); the curves are best fits to the data using the pinned Fickian diffusion model. From bottom to top, annealing times are unannealed, 5.0 h, 10.4 h, and 23.4 h. Annealed data are displaced upwards from the unannealed data by increasing factors of 10 for clarity. Data are from sample set B discussed in the text.

The measurements were made on the Surface Profile Analysis Reflectometer (SPEAR) at the Manuel Lujan Nr. Neutron Scattering Center (MLNSC) at the Los Alamos Neutron Science Center (LANSCE). The beam at LANSCE is produced by spallation of neutrons from a tungsten target using a pulsed beam (20 Hz) of 800-MeV protons. The energy spectrum of the neutrons was softened using a liquid-hydrogen (20 K) moderator. The reflectivity (R) curves were collected as a function of the time of flight from the moderator to the detector for a fixed angle of incidence of neutrons on the sample. The detector-to-moderator distance is 12.38 m to give a range of neutron wavelengths of 2–16 Å without the occurrence of frame overlap. By using SPEAR's frame overlap chopper, a second frame may be measured from 16 to 32 Å. However, for the current set of experiments only the 2–16-Å frame was used. Typically, the angle of incidence was chosen to be $\sim1°$ in order to include both the critical edge and reflectivities with reasonable statistics at values of $R\approx10^{-5}$. Typical counting times for these samples were 60 min. The reflected neutrons were counted using an Ordela model 1202 N linear-position-sensitive ^{3}He detector. The data were reduced and plotted as reflectivity versus the perpendicular momentum transfer Q_z, as shown in Fig. 1. The perpendicular momentum transfer is defined as $Q_z=(4\pi/\lambda)\sin\theta$, where λ is the wavelength of the neutrons and θ is the angle of incidence of the beam upon the sample. The error bars in R are too small to be seen in Fig. 1, and represent the statistical errors in the measurements. The largest σ_R/R at $R=1$ (lowest Q) was $<3\times10^{-8}$ and increased to a maximum of 0.02 for the largest Q value shown. The Gaussian resolution error, σ_{Q_z}/Q_z, was nearly constant over this range with a value of $\sim3\%$. No off-specular data were observed indicating smooth interfaces between the silicon substrate and ^{10}B and between the ^{10}B and ^{11}B.

C. Data analysis

The NR data were fitted using a standard Marquardt nonlinear least-squares-fitting routing. A scattering length density profile was modeled in the following manner. The complex values of the scattering lengths b of ^{10}B and ^{11}B were calculated from their respective purities as $b_{11_B}=(64.9\times10^{-6}-0.280\times10^{-6}i)$ Å and $b_{10_B}=(4.2\times10^{-6}-10.3\times10^{-6}i)$ Å and were used in all subsequent calculations without modification. A model functional form of the atomic number density profile $N(z)$ was parameterized. The scattering length density profile β was calculated for a series of small steps in distance to approximate the smooth functional form of the density profile across the ^{10}B/^{11}B interface for the various models. The scattering length density is defined as $\beta=4\pi\overline{Nb(z)}$, where $\overline{Nb(z)}$ is the average value of the product of the number density N and the coherent neutron scattering length b for each isotope at a given depth z. The resulting reflectivity was then calculated using this stepped profile by iterative reflectance calculations at the interfaces of the small steps,[6] and the parameters were adjusted by the fitting program to minimize the value of χ^2. In each of these fits, all parameters were allowed to vary, and initial guesses were made based on knowledge of the physical properties of the deposited films. These initial guesses were substantially varied in order to approach a global, rather than local minimum in parameter space.

The relevant models used for the density profile of the boron layers on the silicon were standard Fickian diffusion, resistive interfacial diffusion, pinned Fickian diffusion and a step function model that assumes no diffusion at the interface and a constant boron density throughout. A number of functional forms (simple exponential, hyperbolic tangent, etc.) were also tried without success.

The expected model was normal, unobstructed Fickian diffusion at the interface between similar layers. Fick's second law of diffusion for a concentration independent diffusion constant is

$$\frac{\partial C}{\partial t}=D\frac{\partial C^2}{\partial z^2}. \tag{1}$$

In this case, D is the diffusion constant, C is the number density of ^{11}B in ^{10}B, z is the distance from the ^{10}B/^{11}B interface, and t is the time. For convenience of solution, z is defined as zero at the interface. The boundary and initial conditions for $C(z,t)$ for this system are[7]

$$C(0,t)=\frac{C_0}{2},$$

$$C(\infty,t)=C_0 \quad (z>0), \tag{2}$$

$$C(z,0)=0 \quad (z<0),$$

where C_0 is the initial (unannealed) value of the concentration of ^{11}B. The first condition is a result of the assumption that the materials at the interface immediately reach thermal equilibrium, and that there is a single phase involved. The second condition is a simplification that results from assuming a semi-infinite ^{10}B layer, such that full mixing never occurs. This is justified for short annealing times. The third condition is a statement that the density profile is a step function at $t=0$. Under the above boundary conditions, the solution to Fick's law [Eq. (1)] is[7]

$$C(z,t)=\frac{C_0}{2}\left[1+\mathrm{erf}\left(\frac{z}{2\sqrt{Dt}}\right)\right]. \tag{3}$$

The model for the entire system examined consists of a semi-infinite layer of ^{10}B, an interface described by Eq. (3), an undiffused layer of ^{11}B, a rough ^{11}B/vacuum interface, and finally vacuum. Since ^{10}B has a large imaginary component of the scattering length (hence a large absorption cross section), the fits were insensitive to the presence of a silicon substrate in the model; therefore, the silicon substrate has been ignored. This model is referred to as standard Fickian diffusion.

In the pinned model of Fickian diffusion, the interface does not reach a homogeneous equilibrium of 1:1 ^{10}B:^{11}B at the interface. Rather, the concentration of ^{11}B on either side of the interface is fixed, resulting in a discontinuity at the interface described by the parameter k. Fick's law applies, but the boundary conditions require that the ratio of the concentration of ^{10}B to ^{11}B is held constant at $z=0$. The flux of atoms into and out of the interface is again equal. The boundary conditions then become[8]

$$k=\frac{C_2}{C_1} \quad (z=0),$$

$$D_1\frac{\partial C_1}{\partial z}=D_2\frac{\partial C_2}{\partial z} \quad (z=0), \tag{4}$$

where C_1 is the concentration of ^{11}B on the initial ^{11}B side of the interface, and C_2 is the concentration of the ^{11}B on the initial ^{10}B side of the interface. By setting the diffusion constants D_1 and D_2 equal, since each represents diffusion for elemental boron, the solutions to Eq. (1) under these boundary conditions are[8]

$$C_1(z,t)=\frac{C_0}{1+k}\left[1+k\ \mathrm{erf}\left(\frac{z}{2\sqrt{Dt}}\right)\right] \quad (z>0),$$

$$C_2(z,t)=\frac{kC_0}{1+k}\left[1-k\ \mathrm{erf}\left(\frac{|z|}{2\sqrt{Dt}}\right)\right] \quad (z<0). \tag{5}$$

This model creates an invariant discontinuity in the function at the interface, and is referred to as pinned Fickian diffusion.

In the resistive model for interfacial diffusion,[8] a similar nonunitary ratio of isotopes occurs at the interface, but the composition at the interface varies as a function of annealing time. Although we could obtain reasonable fits with this model, the resulting parameters were inconsistent and unphysical. Consequently, this model was determined to be less applicable to this system, and will be discussed only briefly in Sec. III.

TABLE I. Best-fit results from sample set A (Ref. 4) using the pinned Fickian diffusion model.

Annealing time (h)	Number density ($Å^{-3}$)	Air/^{11}B roughness (Å)	^{11}B thickness (Å)	k	$\sqrt{Dt}$ (Å)	D ($cm^2\ s^{-1}$)/10^{-17}
0.0	0.1113±0.0003	11.3±3.9	646±31	1[a]	8±3	b
2.4	0.1176±0.0002	11.4±0.7	627±20	0.45±0.07	24±2	0.7±0.1
5.4	0.1171±0.0003	12.4±0.6	628±28	0.37±0.04	38±3	0.7±0.1
9.7	0.1182±0.0003	12.6±0.7	628±40	0.36±0.03	49±4	0.7±0.1
22.3	0.1185±0.0003	10.2±0.9	619±80	0.36±0.02	96±8	1.2±0.2
35.4	0.1179±0.0003	13.1±0.8	617±5	0.41±0.02	123±1	1.2±0.1

[a]Fixed in the fitting routine.

[b]Not applicable for the unannealed sample.

III. RESULTS AND DISCUSSION

A. General observations

All density profiles used produced fits that were insensitive to the presence of a silicon layer in the model; thus any neutrons were either reflected off the boron prior to hitting the silicon or absorbed by the ^{10}B either before or after reflection from the silicon/^{10}B interface. No significant off-specular intensity was observed indicating a smooth interface between the ^{10}B and ^{11}B. Furthermore, diffusion in samples annealed at 360 °C and for stated times converged to less than 650 Å in our models, the thickness of the thinnest films. Consequently, consideration of boron-atom diffusion into the silicon, or backdiffusion from the Si/^{10}B interface or from the surface was not considered. We also examined samples annealed at 400 and 520 °C, but for the shortest annealing times used (less than 30 min) ^{10}B was observed at the surface, indicating mixing of the films through the entire ^{11}B layer thickness. The 1-h anneal at 400 °C proceeded as far as or further than the 35.4-h anneal at 360 °. In order to analyze any of the 400 °C or higher-temperature data, new boundary conditions must be applied to Eq. (1) to model the case of diffusion to the boundary and backdiffusion, which is beyond the scope of this paper. All detailed analyses were thus restricted to the 360 °C anneals.

For all unannealed samples, the step-function model provided excellent fits to the data, and required a roughness at the ^{11}B/^{10}B interface of less than 12 Å. The step-function results of the unannealed samples can be found in Tables I and II. A step function did not fit any of the annealed samples.

B. Results from diffusion models

The pinned Fickian diffusion model produced excellent fits to the reflectivity data for all anneal times of sample set B. Figure 1 shows the reflectivity data and the corresponding pinned Fickian fit for this data set. Note that the oscillations in the reflectivity curve are followed by the fit up to the highest Q_z measured. Figure 2 shows the density profiles that resulted in these fits. Notice that the ratio C_2/C_1 at the interface ($z=0$) is constant for each of the anneals, and results in a steplike discontinuity.

Conversely, the standard Fickian model did not fit the reflectivity data of set B. This result is consistent with that observed[4] on the sample set A. The standard Fickian model adequately reproduces the peaks at low-Q_z values, but dramatically damps them at higher values of Q_z. The inability of the standard Fickian model to describe the diffusion adequately was explained[4] by considering the large-Q_z approximation of the expression for the reflectivity,[6,9]

$$R(Q_z)=\frac{(4\pi)^2}{{Q_z}^4}\left|\int_{-\infty}^{\infty}\frac{db}{dz}\,e^{iQ_z}dz\right|^2. \tag{6}$$

As Eq. (6) indicates, the reflectivity may be approximated by the square of the Fourier transform of the derivative of the scattering length density. Consequently, the fact that the observed reflectivity at high Q_z oscillated with a greater amplitude than predicted by Eq. (3) implies that sharper features in the scattering length density profile are needed to provide higher harmonic content to the reflectivity curves. The sharp discontinuity at the interface in the pinned Fickian model satisfies this requirement, and gives a significantly better fit to the reflectivity data.

The resistance model also has a step at the interface, but no physically consistent parameters were obtained upon fitting the data. The diffusion constant varied by several orders of magnitude for a given temperature, and the interfacial resistance also changed dramatically. Furthermore, the value for the ratio of boron isotopes at the interface did not tend

TABLE II. Best-fit results from sample set B using the pinned Fickian diffusion model.

Annealing time (h)	Number density ($Å^{-3}$)	Air/^{11}B roughness (Å)	^{11}B thickness (Å)	k	$\sqrt{Dt}$ (Å)	D ($cm^2\ s^{-1}$)/10^{-17}
0.0	0.1125±0.0009	16.7±0.4	711±3	1[a]	4.6±0.4	b
5.0	0.1152±0.0010	11.4±0.3	701±10	0.55±0.14	51±1	1.48±0.06
10.4	0.1158±0.0010	11.4±0.2	699±10	0.61±0.09	69±1	1.28±0.04
23.4	0.1155±0.0017	10.9±0.2	698±14	0.63±0.08	91±2	0.98±0.03

[a]Fixed in the fitting routine.

[b]Not applicable for the unannealed sample.

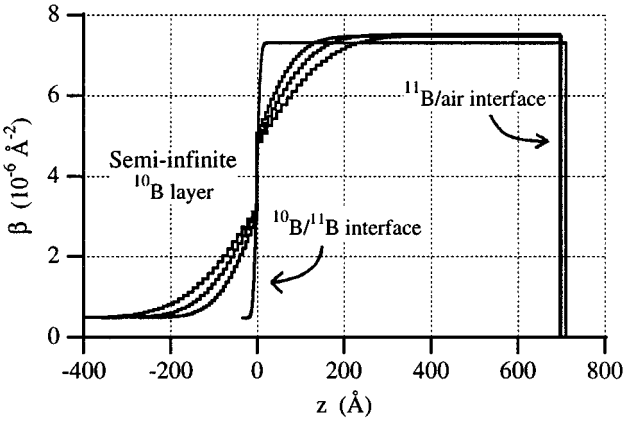

FIG. 2. Density profiles from sample set B produced from the parameters of the best fit to the reflectivity curves shown in Fig. 1. The scattering length density β (which is directly related to the concentration of ^{11}B) is plotted vs the distance from the ^{10}B/^{11}B interface z. Annealing times from top to bottom ($z>0$): unannealed, 5.0 h, 10.4 h, and 23.4 h.

toward a homogeneous composition. Although there may be some resistance at the interface due to a small difference in thermodynamic potential between ^{10}B and ^{11}B, the apparent fixed composition at the interface seems to have a larger effect.

The parameters resulting from the fits to the pinned Fickian model of Eq. (5), and the resulting real portion of the scattering length density profiles for set A, Re$[b(z)]$, are shown in Ref. 4. Table I summarizes those results; the best-fit values corresponding to the number density of atoms (the same value was used for both ^{11}B and ^{10}B), the air/^{11}B interface roughness, the total thickness of the outer layer, the value of k (the ratio of C_{10_B} to C_{11_B} at the interface), $\sqrt{Dt}$ (which equals the Gaussian resolution parameter σ at the ^{11}B/^{10}B interface), and the diffusion constant for each annealing time. Also listed in Table I are the values of the parameters for the fit to the unannealed sample by fixing the value of $k=1$. For this case, Eq. (6) reduces to Eq. (3).

Several conclusions may be drawn upon examination of Table I. First, there was an initial density change of $\sim$6% between the unannealed sample and the 2.4-h annealed sample. Thereafter, the density remained constant. This is consistent with the layer thickness change (<3%) as well. The interface did not move significantly after the first desification, thus confirming the assumption that the diffusion constants of ^{10}B and ^{11}B are equal within the given errors. Also, note the interface broadened to the entire thickness of the original ^{11}B layer by the 35.4-h anneal. Finally, from Table I, a consistent set of values is observed for the diffusion constant, although the 35.4- and 22.3-h annealed samples have slightly different values than the shorter anneals. This difference, although statistically insignificant, may be due to inadequacies in the model at long annealing times, or to the fact that these two samples were annealed twice, and thus subjected to heating and cooling twice. Nevertheless, the values obtained for the diffusion constants are all consistent with measurements on other amorphous systems.[10,11]

Table II shows the comparable results for the fits to the pinned Fickian model of diffusion for sample set B, which had minimal time between boron depositions. Again, the sample density increases ($\sim$2%) with a corresponding small decrease in film thickness (<2%) upon the first anneal, but remains constant afterwards. This result is graphically illustrated in the density profiles of Fig. 2. The observed value of k was 0.60 ± 0.06, which while consistent for the sample set B is different than the observed k for sample set A, the value being 0.30 ± 0.02. Since each set is self-consistent, the different sample preparations must have resulted in slightly different film properties and interfaces. Sample set B's higher k value is closer to the standard Fickian value of $k=1$, which implies a smoother interface than set A. This result is consistent with the preparation of set B, which was under better controlled conditions.

In sample A, we first considered that the short delay, occurring between the deposition of the first layer and second layer of boron, allowed contaminants to adsorb at the interface or gave the surface sufficient time to reconstruct. Small amounts of extraneous materials may have formed stoichiometric compounds, for example, B_2O_3, with fixed percentages of ^{10}B and ^{11}B, at the time of deposition or after the first anneal. At the interface between this extra layer and either the ^{10}B or ^{11}B, a local equilibrium would have been established between the B_2O_3 and pure boron, and as seen in oxide layers on silicon,[12] provided a barrier to 950 °C diffusion for oxide layers larger than about 30 Å. This layer would have pinned the concentration of the boron to the value it would have at the boundary of the two-phase region in the equilibrium phase diagram.[7,13]

However, because the delay time was minimal for sample set B, it is unlikely that contamination plays a role at the interface. The fact that the pinned Fickian model fits the data well suggests that, if a fixed composition layer exists in both sets A and B, it must be very thin; otherwise, it would give rise to additional interference fringes, since peak separations are inversely proportional to film widths. Additionally, the diffusion from the interface preserves the fixed composition throughout the film rather than mixing homogeneously beyond the interface to sandwich a thin, fixed, contaminated layer.

The origin of the fixed composition at the ^{11}B/^{10}B interface and beyond may be better explained by the formation of amorphous boron clusters which do not diffuse at 360 °C, while the interstitial boron atoms are mobile at this temperature. Although the phase diagram for boron is virtually unknown, boron clusters are commonly found in boron-rich solids,[14] and the conditions of transition from disordered clusters to crystalline order in amorphous boron are still under consideration.[15] Theoretical studies of such boron clusters suggest that small stable positive and neutral clusters can exist at room temperature.[16] Amorphous boron is known to have a network of ''soccer-ball'' B_{84} clusters[17] and B_{12} icosahedra, which can cluster in sizes 2–5 nm in diameter,[17] in both films and bulk samples.[18] Although the amorphous boron has a basic structural unit, long-range order is not found until the full metastable, amorphous to crystalline α- or β-rhombohedral transition occurs above 1300 K.[15]

The resulting amorphous material has clusters that are less likely to diffuse than less covalently saturated boron atoms. Each side of the interface has very slowly diffusing boron

atoms (assumed negligible rate) associated with the clusters, and more freely diffusing atoms (less covalently bound) between them. This result is suggested by studies on nanocrystalline Pd (Ref. 19) and on nanocrystalline Ni (Ref. 20), where fast atomic diffusion due to free volumes, cluster boundaries, or grain boundary layers can coexist with slower diffusion processes of the nanocrystals themselves. Consider a weakly associated network of ^{10}B clusters on a weakly associated network of ^{11}B clusters. The interstitial amorphous boron atoms can easily diffuse between the large immobile clusters, while the clusters remain intact. The initial assumption of homogeneity at the interface upon annealing applies to the diffusing atoms, but the stationary clusters pin the composition at the value defined by k. As $t\rightarrow\infty$, the composition is defined by the homogeneous distribution and complete mixing of the mobile atoms between the clusters which will not have changed sides of the interface. This fixed composition throughout the sample is then also described by the parameter k, which initially described only the interface.

The amorphous boron film may be deposited with these clusters intact, or the clusters may be a result of annealing since the density increased after the first anneal, and remain constant afterwards. Either effect is consistent with the results. However, once the clusters have formed and/or slightly rearranged (the initial effect of annealing), the cluster size and number do not change upon subsequent anneals, as the observed k is consistent for each set. This result is consistent for both sets A and B, although differences in the sample preparations led to a slightly smaller k (less ideal) of sample A. Different heating and cooling rates have a significant effect on the crystallinity of boron samples, at least at higher temperatures.[15] The measured difference in k between the sample sets A and B could be a result of a different amount of cooling between depositions due to the different delays, set A having more cooling, more clusters and thus a lower k (farther away from the ideal standard of $k=1$). This difference in k then is a function of delay time, and is consistent with our present theory of cluster formation moving the interface farther from ideal.

C. Comparison of the standard and pinned Fickian models

Clearly the results indicate that the interface between the two amorphous layers behaves differently than expected from homogeneous boron diffusion. Although the standard Fickian model did not fit the data, a discussion of the resulting diffusion coefficient D is useful, since the pinned Fickian model seems to fit the self-diffusion of amorphous boron rather than the expected model. Does a significant and measurable difference in D result from using the different models? What parameters in the models most affect the observed diffusion constant? And what is the range of parameters important in differentiating D?

In order to independently test our model of pinned Fickian diffusion, we examined the same sample sets A and B by neutron depth profiling[21] (NDP), a direct measurement of ^{10}B concentration for thicknesses up to a few micrometers. These NDP results[22] were inconclusive in verifying the applicability of one model over the other. The main reason for the inability to distinguish between the two models is the high sensitivity of the profile to the resolution function of the energy detector, which directly affects the measurement of the distance traveled.

A step function (which represents the unannealed boron density profile) convoluted with a Gaussian (which represents the resolution function) gives a mathematical error function. Consequently, a pinned Fickian profile can be made to look identical to a standard Fickian profile merely by convoluting it with a Gaussian resolution function. The ''smearing'' effect of such resolution on the sharpness of the interface and the interdependence of the parameters k and $\sqrt{Dt}$ make it impossible to obtain fit values for these variables with uncertainties smaller than their values. We could obtain excellent fits by fixing k or $\sqrt{Dt}$ to the parameter obtained by neutron reflectivity, and letting the other parameters vary. The complementary parameter converged to the NR value within these large uncertainties.

Clearly, with a technique such as NR, that has high resolution and that is greatly influenced by the ''steepness'' of the density profile due to the nature of the inverse problem, the shape of the density profile has a tremendous influence. However, given direct measurements such as NDP, SIMS, or Rutherford backscattering, the limited resolution is insufficient to distinguish between the two models. The measured diffusion constant varies significantly for the two models, depending on the Gaussian resolution parameter σ and the anneal time. In order to address the applicability of each of the two diffusion models, we examined the application of each model on the experimental NR data and the resulting difference in calculated diffusion constants in the absence of a significant resolution restriction.

D. Comparison by ratio of diffusion constants

Determining an accurate diffusion constant D requires a knowledge of the governing equations for a given experimental system. The calculated diffusion constant depends on the diffusion model used to fit the data. Since many standard methods for determining diffusion constants are to take measurements of concentration at various distances from the interface for different annealing times, we compared the effect of choosing separate models on the resultant D value for our experimental data. The standard and pinned Fickian models might be expected, in some cases, to yield the same diffusion constant, within experimental uncertainty, where the ratio of D_{standard} to D_{pinned}, D_s/D_p, is 1. In such a situation, the distinction between the two models is of little practical value. In the case of the system studied, which we have shown to be governed by pinned diffusion, D_p could be approximated by using the simpler standard Fickian model to calculate D_s. Whether such an approximation is justified would conceivably depend on the thickness of the sample, how long it was annealed, and the care with which it was prepared, among other parameters. Given the resolution of most experimental techniques, the ratio of diffusion constants must be nearly an order of magnitude to be significant. Having a quantitative measure of when it is necessary to discriminate between the two models when calculating diffusion constants would be valuable.

The ratio described above, D_s/D_p, proves to be a useful measure for determining the applicability of the standard

Fickian model. Furthermore, we chose to plot the ratio D_s/D_p as a function of k, so that the effect of decreasing sample deviation from ideal Fickian behavior ($k=1$) could be shown. Solving Eqs. (3) and (5) for the respective diffusion constants, and taking their ratio, yields

$$\frac{D_s}{D_p}=\left(\frac{\text{erfinv}\left(\frac{C(1+k)-C_0}{C_0 k}\right)}{\text{erfinv}\left(\frac{2C}{C_0}-1\right)}\right)^2, \tag{7}$$

where the inverse error function, $y=\text{erfinv}(x)$, satisfies $x=\text{erf}(y)$. Notice that both time and distance cancel in the setting up of the equations in this manner. As shown below, this calculation can be made directly from the measured experimental values of C and C_0, and a known or approximate value of k. The parameters of a given experiment or the specific value of k are not required for the calculation, making it a convenient tool to compare the results of these two models. In the context of the current system, where it has been shown that the data are best fit by the pinned model, D_p is assumed to be the more accurate of the two diffusion constants.

The calculation and interpretation of D_s/D_p was accomplished as follows. For a given annealing time and sample preparation (sets A or B), the experimental value of C (concentration of ^{11}B on the original ^{11}B side) was taken from the pinned Fickian density profile at a given distance from the ^{10}B/^{11}B interface. This value was combined with the experimental value of C_0 (the original concentration of ^{11}B on the original ^{11}B side) and substituted into Eq. (7), yielding D_s/D_p as a function of k. Thus on the D_s/D_p vs k graph only one point, that where k equals the value obtained in the fit, describes our particular system. For any experimental values of distance and concentration, the substitutions essentially force the standard Fickian diffusion constant to increase or decrease relative to the pinned diffusion constant in order to pass through the same point on the density profile. Plots of D_s/D_p vs k using values of C and C_0 from various combinations of annealing time and distance from the interface were made for both sets A and B. Representative plots from set B are shown in Fig. 3.

As the figure indicates, all graphs approach a ratio of 1 in the limit as $k\rightarrow 1$. This result is expected, since Eq. (5) reduces to Eq. (3), and the models converge to a single diffusion constant. It is less intuitive as to why the graphs reach zero at different values of k. From an inspection of Eq. (7), this result occurs when $C(1+k)=C_0$, when D_p becomes infinity. The physical reason for this behavior is as follows. Take, for example, the annealing time of 10.4 h from sample set B, for which the scattering length density at 50 Å was 6×10^{-6} Å^{-2}. This corresponds to both a concentration C and a particular point on the density profile as shown in Fig. 2. For values of k closer to 1, both the pinned profile shown and the standard profile without the discontinuity at the interface will curve up to pass through the point. Since the pinned profile begins at the interface at a higher concentration, it flattens out more than the standard model, yielding a higher diffusion constant. Hence D_s/D_p is less than 1. As k decreases, however, the discontinuity widens. Eventually, the pinned model will be forced to start at the interface with a concentration that corresponds to a scattering length density of 6×10^{-6} Å^{-2}. At this point, the pinned profile will be a flat line, indicating instant and complete diffusion, which is represented by an infinite diffusion constant. Since D_p becomes infinite at this value of k, where $k=(C_0/C)-1$, the ratio becomes zero. Values of the ratio at lower k have no physical meaning; the large discontinuity forces the pinned profile to curve downward to pass through 6×10^{-6} Å^{-2}, which creates an unrealistic density profile that is not observed in experiment.

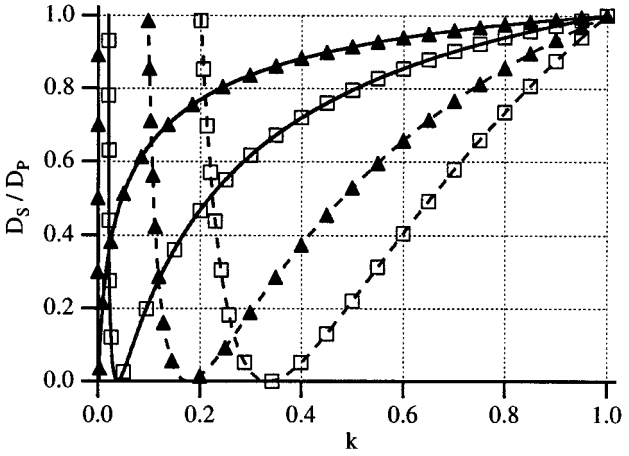

FIG. 3. Graphs of theoretical $D_{\text{standard}}/D_{\text{pinned}}$ vs k for different measured annealing times and distances from the ^{10}B/^{11}B interface for the set B samples. The line style indicates distance from interface: solid, 200 Å; dashed, 50 Å. Symbols indicate annealing time: filled triangles, 5 h; open squares, 23.4 h.

Examination of the graphs in Fig. 3 with a known or approximated value of k will easily give the magnitude of D_s/D_p. In many applications, such as the study of alloys, the value of k is fixed by the composition of the alloy, and is known beforehand. In other cases, the ratio graph looks like the 5-h anneal at 200 Å in Fig. 3 (filled triangles, solid line), where the value of D_s/D_p is nearly constant for a large range of k. In this circumstance, it is likely that an estimate of k will be sufficient to calculate D_s/D_p. For the boron system studied, the ratios of D_s to D_p were determined using the best-fit values from k from each sample set. As discussed previously, these were 0.6 and 0.39 for sets B and A, respectively. The results of this analysis on the curves in Fig. 3 are presented in Table III.

As expected, the difference in diffusion constants increases with annealing time. Both models give a step func-

TABLE III. Ratio of D_{standard} to D_{pinned} (D_s/D_p) as a function of annealing time t and distance from the ^{11}B/^{10}B interface z. The value in parentheses is from set A data; all other values are from set B. The value of the ratio can be interpreted as one minus the error in D_s when used to approximate D_p.

t (h) / z (Å)	5.0	23.4
50	0.66 (0.50)	0.40
200	0.94	0.85

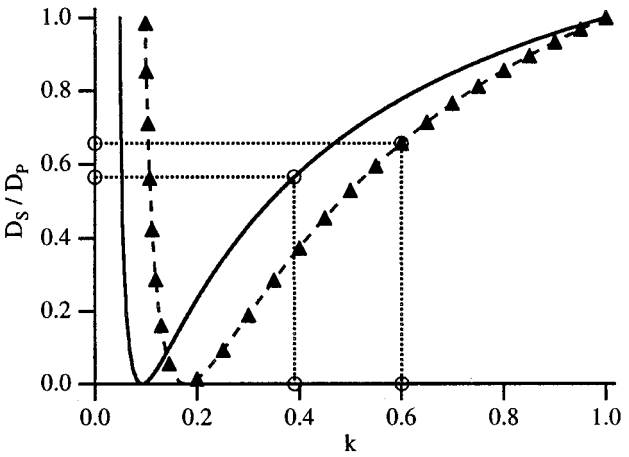

FIG. 4. Graphs of $D_{\text{standard}}/D_{\text{pinned}}$ vs k comparing the two sample sets A and B. The dashed line with filled triangles is the $z=200$ Å, $t=5$ h plot from Fig. 3 (set B). The solid line is the equivalent plot from set A with the same values for z and t. The open circles highlight the difference in D_s/D_p between samples due to their unequal k values.

tion in the limit as annealing time goes to zero, but, as time increases, the models diverge. This effect is less noticeable at larger distances, for the simple physical reason that it takes longer for particles to diffuse the longer distance, so diffusion-related differences are not as exaggerated. The inverse of this is also true; at short distances, diffusion-related effects are exacerbated. Consequently, the ratio decreases by almost 50% in some cases when the distance to the interface is decreased by 150 Å. The ratio also decreases when k is less ideal as a result of different sample preparation. As shown in Fig. 4 and included in Table III, the data from set A gave a value for D_s/D_p that was 24% less than the ratio from set B, with the same annealing time and distance to the interface.

As indicated in Fig. 5, the difference in diffusion constants is less than an order of magnitude for the majority of the range of k values. Indeed, the largest discrepancy that we studied was only a factor of 2.5. For most high-resolution methods of determining diffusion constants, including neutron depth profiling, Rutherfordback scattering, and secondary-ion-mass spectroscopy, any difference under an order of magnitude is not significant. Since the practical differences between the standard and pinned diffusion models are not discernible using these methods, there has been no need for discussion of the pinned model as applied to self-diffusion in solids. However, we have shown that neutron reflectivity possesses the necessary resolution to distinguish between the two models. As a result, for the self-diffusion of amorphous boron, pinned Fickian diffusion is clearly a more applicable model than the traditional standard Fickian model at the temperature studied.

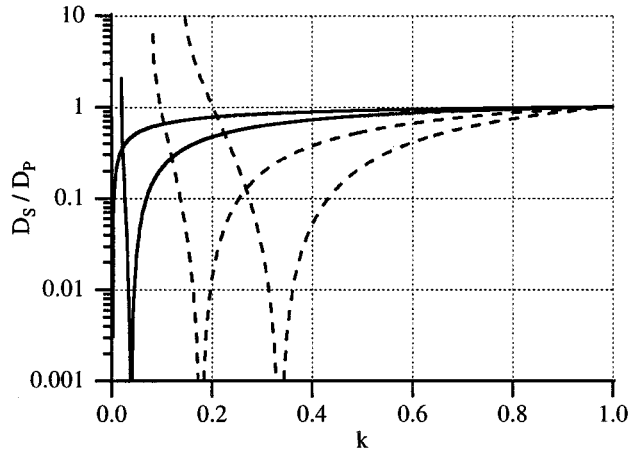

FIG. 5. Data from Fig. 3 plotted on a log scale illustrating the range over which the diffusion constants from the pinned and standard models vary by an order of magnitude or greater ($D_s/D_p<0.1$).

As the resolution of experiments continues to increase, the pinned Fickian model may need to be considered when measuring diffusion constants in amorphous materials. It has already been shown that the choice of model affects the accuracy of D. Using the standard Fickian model to approximate the pinned model also affects the consistency of results. We have shown that the ratio D_s/D_p, and hence the value of D_s, depends on the distance from the interface where concentration data are taken. Consequently, any method that takes data at an arbitrary distance from an interface will yield inconsistent values for the diffusion constant, unless the correct model is utilized. Although these differences are less than an order of magnitude, which is currently insignificant on an experimental scale, we believe that as resolution is enhanced it may be necessary to use the pinned model to obtain consistent and accurate results if this same phenomenon is observed in other amorphous systems.

IV. CONCLUSIONS

We have shown that the contrast between two different isotopes of the same material allows measurement of the detailed shape of the density profile at the interface using neutron reflectometry. From an analysis of the profiles, the diffusion constant, information about the interface between the two isotopes, and the position of the interface with respect to the surface of the material were obtained. A relatively simple model system, self-diffusion of boron, was found not to follow standard Fickian diffusion, i.e., simple error function behavior, but instead had a discontinues density profile at the interface boundary. It is not yet known what effect this result may have on the diffusion of boron from passivating diboride layers.

The pinned composition at the boundary was a different self-consistent value for each of two different sample preparations, indicating that the sample preparation varied somewhat in the two sample sets. Although the source of this pinning is not completely understood, the density profile measurements suggest that the boundary layer, perhaps boron clusters, is stable at 360 °C, and does not break down or shift position during the anneals. In fact, the clusters may have been formed by the 360 °C anneal, and remained intact thereafter. Furthermore, this temperature may be just below a significant phase transition in amorphous boron, since we observed a dramatic difference in the diffusion properties at our shortest anneal time at 400 °C. The measured diffusion constants at 360 °C are inconsistent with the high melting

temperature of elemental boron, but are consistent with measured boron diffusion constants in other amorphous thin films.[10]

The reflectivity measurements give information about the density, but not the structure of the film responsible for that density. The small size of the clusters and the unconventional geometry of the films makes x-ray diffraction elusive. Performing reflectivity studies on known crystalline or polycrystalline samples of $^{11}B/^{10}B$ would be helpful in determining the effect of nanocrystals or clusters on the self-diffusion of boron. Furthermore, annealing to very long times could be used to verify that the nanocrystallinity was consistent throughout the sample and not limited to the interfacial region. If the amorphous boron is comprised of homogeneously distributed nanocrystals, the final boron density profile will be a constant density of ^{11}B to the interface and the complement on the other side of the interface. Although there may be some additional resistance at the interface due to a small difference in thermodynamic potential between ^{10}B and ^{11}B, the apparent fixed composition seems to have a larger effect at 360 °C. No one to our knowledge has ever measured the miscibility of the two boron isotopes, and this technique may be the first with the ability and resolution to do so.

The implications of a pinned interface for the calculation of a diffusion constant vary depending on both the location of concentration measurement z and the anneal time t. The ratio of D_s/D_p, and thus the difference between interpreted diffusion constants, is less ideal as k increases, as the measurement is taken closer to the interface and as the anneal time increases. For measured values of k of 0.6 and 0.39 in our amorphous boron systems, the diffusion constant ratios for the 5-h anneals, using concentration data taken 50 Å from the interface, were 0.66 and 0.50, respectively. Clearly, the choice of diffusion models can have a significant effect on the calculated diffusion constant.

ACKNOWLEDGMENTS

We would like to thank the United States Department of Energy for funding under Contract No. W-7405-ENG-36 with the University of California. S.M.B. acknowledges generous support from the Luce Foundation. This research was supported in part by an award from Research Corporation.

*Present address: Department of Chemistry, Harvey Mudd College, Claremont, CA 91711.

[1] C. S. Choi *et al.*, J. Electrochem. Soc. **138**, 3062 (1991).
[2] A. Kaloyeros, M. Hoffman, and W. S. Williams, Thin Solid Films **114**, 237 (1986).
[3] H. O. Pierson and A. W. Mullendore, Thin Solid Films **95**, 99 (1982).
[4] G. S. Smith *et al.*, Proc. SPIE **1738**, 246 (1992).
[5] F. La Via, K. T. F. Janssen, and A. H. Reader, Appl. Phys. Lett. **60**, 701 (1992).
[6] T. P. Russell, Mater. Sci. Rep. **5**, 171 (1990).
[7] J. D. VerHoeven, *Fundamentals of Physical Metallurgy* (Wiley, New York, 1975), Chap. 6.
[8] J. Crank, *The Mathematics of Diffusion* (Clarendon, Oxford, 1975).
[9] See, for example, J. Leckner, *Theory of the Reflection of Electromagnetic and Particle Waves* (Nijof, Dordrecht, 1987).
[10] D. Gupta, in *Thin Films: The Relationship of Structure Properties*, edited by C. R. Aita and K. S. Streemarsha, MRS Symposia Proceedings No. 47 (Materials Research Society, Boston, 1985).
[11] B. Cantor and R. W. Cahn, in *Amorphous Metallic Alloys*, edited by F. E. Luborsky (Butterworths, London, 1983).
[12] A. D. Sadovnikov, Solid-State Electron. **34**, 969 (1991).
[13] W. Jost, *Diffusion in Solids, Liquids, Gases* (Academic, New York, 1960), pp. 20–26.
[14] E. L. Muetterties, *The Chemistry of Boron and its Compounds* (Wiley, New York, 1967), pp. 29–53.
[15] N. E. Solov'ev, V. S. Makarov, and Ya. A. Ugai, J. Less-Common. Methods **117**, 21 (1986).
[16] R. Kawai and J. H. Weare, J. Chem. Phys. **95**, 1151 (1991).
[17] K. Kimura, Mater. Sci. Eng. B **19**, 67 (1993).
[18] R. Mosseri and J. F. Sacod, in *Structure and Bonding in Non-Crystalline Solids*, edited by G. E. Walrafen and A. G. Revesz (Plenum, New York, 1986), p. 45.
[19] H.-E. Schaefer *et al.*, Nanostruct. Mater. **6**, 869 (1995).
[20] B. S. Bokstein, H. J. Bröse, L. I. Trusov, and T. P. Khvostantseva, Nanostruct. Mater. **6**, 873 (1995).
[21] R. G. Downing, G. P. Lamaze, and J. K. Langland, J. Res. Natl. Inst. Stand. Technol. **98**, 109 (1993).
[22] S. M. Baker *et al.*, in *Neutron Scattering in Materials Science*, edited by D. A. Neumann, T. P. Russell, and B. J. Wuensch, MRS Symposia Proceedings No. 376 (Materials Research Society, Pittsburgh, 1995), p. 79.